Chapter 5

Constraining warm dark matter power spectrum using the cross-correlation of Lyman-α forest and the 21 cm signal*

5.1 Introduction

The ΛCDM model has been widely accepted as the standard model of cosmology with strong support from CMBR observations [207], Galaxy surveys [208] and other cosmological and astrophysical probes. However, several fundamental questions remain unanswered. While, one is still unsure about the actual physical nature of cold dark matter, there is a major discrepancy between the observed abundance of dwarf galaxies in the local group in comparison to a far greater number predicted by CDM simulations. The number of dwarf galaxies observed in voids are also seen to be much lesser than predictions from CDM models [209–212]. There has also been some difference between the observed shallow rotation curves and the ones obtained from CDM simulations which typically produces a cuspy inner density profile [213, 214]. The proposal of Warm dark matter (WDM) attempts to explain some of these discrepancies of the cold dark matter models. Dark matter particles with velocities in the transition zone between relativistic and non relativistic region

*This chapter is based on the paper *Constraining warm dark matter power spectrum using the cross-correlation of HI 21 cm signal and the Lyman-α forest*, Anjan Kumar Sarkar, **Ashis Kumar Pal**, Tapomoy Guha Sarkar, Journal Journal of Cosmology and Astroparticle Physics, 2019, 12, pp 058

are characterized as 'warm'. Mass of the WDM particle falls in region between eV to GeV and are fiducially assumed to be in the keV range [215–218]. Gravitinos and sterile neutrinos are some of the proposed candidates for warm dark matter [218–220]. Unlike CDM, WDM can only cluster on a scale greater then its Jeans scale.

Warm dark matter particles are known to remain relativistic at early times. However their density fluctuations are suppressed owing to free streaming on the scales which are comparable to the horizon size at those epochs. This leads to a consequent suppression of the power spectrum on small scales. At later times the WDM particles undergo cooling due to cosmic expansion and their late time behaviour mimics the CDM with some residual velocity dispersion [220–222]. It is evident that lighter WDM particles shall remain relativistic for longer time and thereby have a larger free-streaming scale. Consequently the formation of halos of mass M_{fs} with $M_{fs} \propto (m_{\rm WDM})^{-\chi}$ shall be suppressed, where χ is some positive parameter. The free streaming of warm dark matter particles manifests through the modification of the matter transfer function.

We have been considering the intensity mapping of the collective HI 21-cm radiation emission from the post-reionization era which as we have established, is believed to provide invaluable information regarding the large scale matter distribution, and expansion history of the Universe [223–227]. Several radio telescopes like the Giant Metrewave Radio Telescope* (GMRT)[228], the Ooty Wide Field Array (OWFA)[229, 230], the Canadian Hydrogen Intensity Mapping Experiment†(CHIME) [231], the Meer-Karoo Array Telescope‡ (MeerKAT), and the Square Kilometer Array (SKA)§ have dedicated goals towards detecting the cosmological HI signal. In earlier chapters we have also noted that a major challenge towards detecting the signal is however posed by large galactic and extra-galactic foregrounds [17]. Several other observational errors like calibration errors and man made radio frequency interferences make it further difficult for the signal to be detected. A statistical detection of the signal with high SNR involves very careful noise analysis and subtraction of foregrounds [17, 232–234].

In previous chapters we have also seen that the diffuse HI from the post reionization epoch can also be mapped out using the distinct absorption features in Lyman-α forest, which traces out the HI density fluctuations along one dimensional

*http://www.gmrt.ncra.tifr.res.in/
†https://chime-experiment.ca/
‡https://www.ska.ac.za/gallery/meerkat/
§https://www.skatelescope.org/

sight lines of background QSOs. The Lyman-α forest observations are known to have numerous applications in cosmological investigations like the measurement of matter power spectrum [235–237] and the bispectrum [238, 239], estimation of cosmological parameters [240, 241], constraining reionization history [242] and modelling of dark energy [243] etc. Different sources of observational error pertaining to the Lyman-α observations arise mainly from improper modelling and subtraction of the continuum, improper modelling and inclusion of the fluctuations of the ionizing source, uncertainties in the temperature-density relation in the IGM [244–246] and metal line contaminations [247]. The Baryon Oscillation Spectroscopic Survey (BOSS) aims to use the imprint of BAO in the Lyman-α forest as a probe of dark energy. The present catalog of SDSS [208] indicates the availability of a large number of QSO spectra with high signal to noise ratio (SNR). This allows us to do a 3-dimensional analysis of the Lyman-α forest and thereby improve the constraints on cosmological parameters.

The cross-correlation of the Lyman-α and 21-cm signal has been ascertained by both linear analysis [248] and robust numerical simulations [100]. The cross-correlation technique has been proposed to be a way to bypass some of the major observational issues [248]. There also has been the proposal of cross-correlating the 21-cm signal with the Lyman break galaxies [21]. A successful detection of the HI 21-cm emission at redshift $z \sim 0.8$ using cross correlations of HI 21-cm maps and galaxies has been reported [249]. The foregrounds which plagues the 21cm observations are expected to pose less severe challenges in detecting the cross-correlation signal as the the foregrounds in HI 21-cm observations appear only as a noise in the cross correlation and can therefore be tackled for a statistically significant detection.

In this chapter we investigate the possibility of measuring warm dark matter mass through the way it affects the cosmological power spectrum. We consider the 3D cross power spectrum of the post reionization HI 21-cm signal and the large scale Lyman-α forest. We discuss the possibility of detecting the cross-correlation signal in a WDM cosmology using future Lyman-α forest surveys with very high QSO number densities and two radio telescopes - the OWFA and the upcoming SKA-mid phase1 (SKA1-mid). These two radio interferometers are chosen for our analysis since they have distinctly different array layouts and observational parameters. We make predictions for warm dark matter masses and the possibility of statistical detection of the suppression effect of WDM on the binned cosmological power spectrum.

5.2 The redshifted HI 21-cm and the Lyman-α forest cross-correlation signal in a WDM cosmology

Warm dark matter suppresses the growth of perturbations on scales that are smaller than the free streaming scale λ_{WDM}. The free streaming scale is found to be inversely related to the WDM mass m_{WDM} as $\lambda_{WDM} \propto m_{WDM}^{-4/3}\Omega_{WDM}^{1/3}$ (which corresponds to a mode $k_{WDM} = 2\pi/\lambda_{WDM}$) [250]. This would lead to an erasure of structures of masses smaller than

$$\frac{4}{3}\pi\lambda_{WDM}^{3}\bar{\rho} \tag{5.1}$$

where $\bar{\rho}$ is the mean background density. The free streaming scale introduces a modification to the CDM matter power spectrum through a suppression in the matter transfer function. The transfer function in the WDM model is related to the CDM transfer function as

$$T_{WDM}(k) = \left[1 + (\alpha k)^{2\mu}\right]^{-10/\mu} T_{CDM}(k) \tag{5.2}$$

where the parameters are obtained from numerical simulations [251] as $\mu = 1.12$ and α is given by

$$\alpha = 0.049 \left[\frac{m_{WDM}}{keV}\right]^{-1.11} \left[\frac{\Omega_{WDM}}{0.25}\right]^{0.11} \left[\frac{h}{0.7}\right]^{1.22} h^{-1}Mpc \tag{5.3}$$

We use the linear transfer function from [252] to compute the WDM power spectrum using the above fit function. The suppression of scales smaller than the free streaming scale, if detected, shall allow us to measure WDM mass. The halo model based non-linear WDM transfer function is discussed in the Appendix.

Following the complex phase transition during the epoch of reionization [253–255], most of HI in the post-reionization era ($z \leq 6$) is believed to be clumped in the highly dense regions that are identified as the Damped Lyman Alpha (DLA) systems in quasar observations. The redshifted 21 cm radiation from individual HI clouds is very weak. However, radio observations in the frequency range 210 MHz $\leq \nu_{\rm HI} \leq$ 1420 MHz holds the potential to tomographically map out the collective diffuse emission from these systems in the post-reionization era.

The CMBR brightness temperature changes from T_γ to $T(\tau_{21})$ under radiative transfer through a HI cloud at redshift z along the line of sight $\hat{\mathbf{n}}$. This is due to the

emission or the absorption associated with the the spin flip Hyperfine transition of HI in its rest frame at frequency $\nu_c = 1420\,\mathrm{MHz}$. The primary quantity of interest in a radio-interferometric observations is the excess brightness temperature $T_b(\hat{\mathbf{n}}, z)$ that is written as (see Eq. 2.7),

$$T_b(\hat{\mathbf{n}}, z) = \frac{T(\tau_{21}) - T_\gamma}{1+z} \approx \frac{(T_s - T_\gamma)\tau_{21}}{1+z}. \tag{5.4}$$

at a redshift z, τ_{21} gives the HI 21-cm optical depth.

The fluctuations in $T_b(\hat{\mathbf{n}}, z)$ is given by $\delta_T(r\hat{\mathbf{n}}, z) = \bar{T}(z) \times \eta_{\rm HI}(r\hat{\mathbf{n}}, z)$, where r is the comoving distance corresponding to z (see Eq. 2.11 and Eq. 2.12).

$$\bar{T}(z) = 4.0\mathrm{mK}(1+z)^2 \left(\frac{\Omega_{b0}h^2}{0.02}\right)\left(\frac{0.7}{h}\right)\left(\frac{H_0}{H(z)}\right) \tag{5.5}$$

and

$$\eta_{HI}(r\hat{\mathbf{n}}, z) = \bar{x}_{HI}(z)\left\{\left(1 - \frac{T_\gamma}{T_s}\right)\left[\delta_H(z, \hat{\mathbf{n}}) - \frac{1+z}{H(z)}\frac{\partial v}{\partial r}\right] + \frac{T_\gamma}{T_s} s\delta_H(\hat{\mathbf{n}}r, z)\right\} \tag{5.6}$$

Here $\bar{x}_{HI}(z)$ is the mean neutral fraction, $\delta_H(z, \hat{\mathbf{n}})$ is the density fluctuations in the HI and the function s relates the fluctuations of the spin temperature with that of the HI density [256]. The peculiar velocity of the gas, v leads to the anisotropic term $(1+z)/H(z)\frac{\partial v}{\partial r}$.

The post reionization epoch is characterized by $T_\gamma/T_s << 1$ owing to rapid rise of T_s at low redshifts, and the 21 cm signal is seen in emission. We then have,

$$\eta_{HI}(r\hat{\mathbf{n}}, z) = \bar{x}_{HI}(z)\left[\delta_H(z, \hat{\mathbf{n}}) - \frac{1+z}{H(z)}\frac{\partial v}{\partial r}\right]. \tag{5.7}$$

The fluctuation $\delta_T(\mathbf{r})$ in Fourier space is denoted by $\Delta_T(\mathbf{k})$ and is given by [248]

$$\Delta_T(\mathbf{k}) = C_T[1 + \beta_T\mu^2]\Delta(\mathbf{k}) \tag{5.8}$$

where $\Delta(\mathbf{k})$ is the Fourier transform of the underlying dark matter over density δ. The peculiar velocity of the gas is assumed to sourced solely by dark matter overdensity leading to redshift space distortion which is quantified through the parameter β_T and $\mu = \hat{\mathbf{n}}\cdot\hat{\mathbf{k}}$. The quantity $C_T(k, z) = \bar{T}(z)\bar{x}_{HI}(z)b_T(k, z)$ gives the amplitude of the fluctuation, where the bias $b_T(k, z)$ relates the HI fluctuations $\Delta_H(\mathbf{k})$ to dark matter fluctuations $\Delta(\mathbf{k})$ through $\Delta_{\rm HI}(\mathbf{k}) = b_T(k, z)\Delta(\mathbf{k})$. Apart from the cosmological parameters, the post-reionization HI is essentially modelled

using two functions $\bar{x}_{HI}(z)$ and $b_T(k, z)$.

The post-reionization HI bias has been extensively studied using numerical simulations [97–99] . Most of these simulations rely on some canonical way to populate the haloes with neutral hydrogen and consequently identify them as DLAs. The HI in halos should have some minimum threshold circular velocity so that it may shield itself from ionizing radiation. This threshold sets a lower bound for the halo mass $M_{\rm min}$. Further, very massive halos also do not contain any HI [257]. The total neutral gas is distributed to halos within a chosen mass range such that the mass of the gas assigned to a halo is proportional to the mass of the halo.

Using this simple scheme it has been found that the HI bias grows monotonically with k on small scales. Some additional scale dependence of the bias is also owes its origin to the fluctuations in the ionizing background. On large scales, the bias is however found to be a constant increasing only with redshift. Noting that our model assumes that bulk of the neutral gas is contained in halos, cosmologies with massive neutrinos and warm dark matter show a greater HI clustering than the model with only cold dark matter. This is because matter fluctuations at smaller scales are wiped out due to the free streaming effect of the warm dark matter and the neutrinos, whereby smaller mass halos are rarer in these models.

The Lyman-α forest traces out the small fluctuations in the HI density in the largely ionized IGM along the line of sight to distant quasars where they manifests as a distinct absorption features in the observed quasar spectra. Whereas the 21-cm signal in the post reionization era is sourced by the dense DLA clouds, the Lyman-α forest is sourced by the tiny HI fluctuations in the predominantly ionized IGM. The transmitted QSO flux through the Lyman-α forest is given by the fluctuating Gunn-Peterson effect as $\mathcal{F} = \bar{\mathcal{F}} e^{-A(1+\delta)^{\Gamma}}$ (see Eq. 3.15) where $\bar{\mathcal{F}}$ denotes the mean transmitted flux, Γ is a parameter dependent on the slope of the temperature-density power law relation, and the parameter $A \sim 1$ has implicit dependence on the astrophysical properties of the IGM and other cosmological parameters. However, on a reasonably smoothed scale, the fluctuation in the transmitted flux $\delta_{\mathcal{F}} = (\bar{\mathcal{F}} - \mathcal{F})/\bar{\mathcal{F}} \propto \delta$. This linear dependency on large scales has been studied and validated by numerical simulations of the Lyman-α forest [100].

In a manner similar to the HI 21-cm signal, the Fourier space fluctuations in the transmitted flux of the Lyman-α forest can be written as,

$$\Delta_{\mathcal{F}}(\mathbf{k}) = C_{\mathcal{F}}(1 + \beta_{\mathcal{F}}\mu^2)\Delta(\mathbf{k}). \tag{5.9}$$

The parameter $\beta_{\mathcal{F}}$ quantifies the anisotropy in $\Delta_{\mathcal{F}}(\mathbf{k})$ in a manner similar to

the redshift space distortion parameter of the HI 21-cm signal β_T. However, the non-linear relation between the Lyman-α transmitted flux and the underlying dark matter density field makes the interpretation of $\beta_{\mathcal{F}}$ different from that of $\beta_{\rm T}$ in that β_F is not to be treated as the bias parameter for the Lyman-α forest. Further, C_T and β_T are independent parameters, but are both dependent on the HI bias b_T, whereas $C_{\mathcal{F}}$ and $\beta_{\mathcal{F}}$ has no such common factor. It has been seen in numerical simulations that fluctuations in the Lyman-α flux can be well described by a linear theory with a scale independent bias on large scales.

We express the three dimensional power spectrum of 21-cm signal, the Lyman-α forest and the cross correlation generally as

$$\langle \Delta_a(\mathbf{k})\Delta_b^*(\mathbf{k}')\rangle = (2\pi)^3\delta^3(\mathbf{k}-\mathbf{k}')P_{ab}(\mathbf{k}) \tag{5.10}$$

where a, b can generally be $\mathcal{F}$ and T. In redshift space, the expression for $P_{ab}(\mathbf{k})$ is is given by

$$P_{ab}(\mathbf{k}) = C_aC_b(1+\beta_a\mu^2)(1+\beta_b\mu^2)P(k) \tag{5.11}$$

where $\mu = k_\parallel/k$, the direction cosine of the wave-vector to the line-of-sight, and $P(k)$ gives the matter power spectrum (this is $P^{\rm WDM}$ in our analysis). The auto-correlation power spectrum corresponds to $a = b$ and the cross-correlation power spectrum corresponds to $a = T$ and $b = \mathcal{F}$.

We have used $C_{\mathcal{F}} = -0.13$ and $\beta_{\mathcal{F}} = 1.58$ for the Lyman-α forest at redshift $z_c = 2.55$ in our analysis. This is obtained from the fit to the 1-D Lyman forest power spectrum [258]. For the HI 21-cm signal, we have used $C_T = (x_{\rm HI}b_{\rm HI}\bar{T}$ and $\beta_T = f(\Omega)/b_{\rm HI}$, where $x_{\rm HI}$, $b_{\rm HI}$, $f(\Omega)$, and $\bar{T}$ respectively are the mean neutral hydrogen fraction, HI bias, linear growth rate of the matter density perturbations, and the characteristic brightness temperature for the HI 21-cm signal [234, 259]. We have used $A_c = C_{\mathcal{F}}C_T$ as the amplitude of the cross correlation power spectrum, and $A_T = C_T^2$ and $A_F = C_{\mathcal{F}}^2$ give the amplitude of the power spectrum of the HI 21-cm signal and the Lyman-α forest respectively.

We have calculated the mean neutral hydrogen fraction $x_{\rm HI}$ using the relation $x_{\rm HI} = \Omega_g/\Omega_b$ where Ω_b and Ω_g refer to the baryon density parameter and the neutral gas density parameter in the universe respectively. DLA observations [260–262] have measured $\Omega_g \sim 10^{-3}$ over a redshift range $1 < z < 5$. This corresponds to $x_{\rm HI} = 0.02$, which we have used in our analysis. Semi-numerical simulations of the post-reionization HI 21-cm signal [97, 263] are found to be consistent with

a scale-independent, linear HI bias at large scales ($k < 1\,\mathrm{Mpc}^{-1}$). However, HI bias becomes highly non-linear as we go down to smaller scales ($k > 1\,\mathrm{Mpc}^{-1}$). We have accounted for this behavior by using a scale and redshift dependent HI bias [99]. The value of $f(\Omega)$ has been calculated using the ΛWDM cosmological parameters given in [207].

5.3 Some observational aspects

We have used the quasar number distribution from the DR14 of SDSS [208]. The quasar distribution is seen to peak at $z = 2.25$, and falls off as we move away from the peak. It is worthwhile to consider the cross-correlation at redshifts near to the peak. This shall enable us to accommodate a large number QSO sightlines thereby reducing the noise contribution arising from the discrete sampling of the QSOs. For the purpose of the present analysis, we have chosen a fiducial redshift of $z_c = 2.55$. For a quasar at z_Q, we note that we eliminate the part of the spectra $10,000$ km s^{-1} blue-ward of the Lyman-α emission peak to avoid the the quasar proximity effect and also consider the part of the spectra that is beyond $1,000$ km s^{-1} red-ward of the Lyman-β line or the O-VI lines to avoid the confusion of the Lyman-α forest with other absorption lines.

For a given quasar, there is a restrictive redshift range for which the quasar spectrum maybe used for cross-correlation. The cross-correlation is also only possible in the region of overlap between this redshift range and the band width of the 21-cm observation. We have considered both complete and partial overlap to estimate the mean quasar number density $n_Q(z_c)$. For the Lyman-α forest, the actual signal to noise ratio (SNR) can be as large as 10. We have adopted an uniform value of $SNR = 5$ for our analysis.

The discussion till now has been restricted to 21-cm observations in a single pointing direction. Typically, the field of view of the radio interferometer is much smaller than the area covered by spectroscopic surveys like BOSS, and it is worthwhile to also consider the possibility of extending the analysis to a situation where 21-cm observations are carried out in multiple pointing directions. In the present work, we assume the cross-correlation signal from each pointing direction to be statistically independent of each other whereby the Fisher matrix for the combined observation is the sum of individual fisher matrices for each pointing directions. It is important to note that for carrying out the cross-correlation, both the Lyman-α and the HI 21-cm signal are to be smoothed at the same resolution. Given that

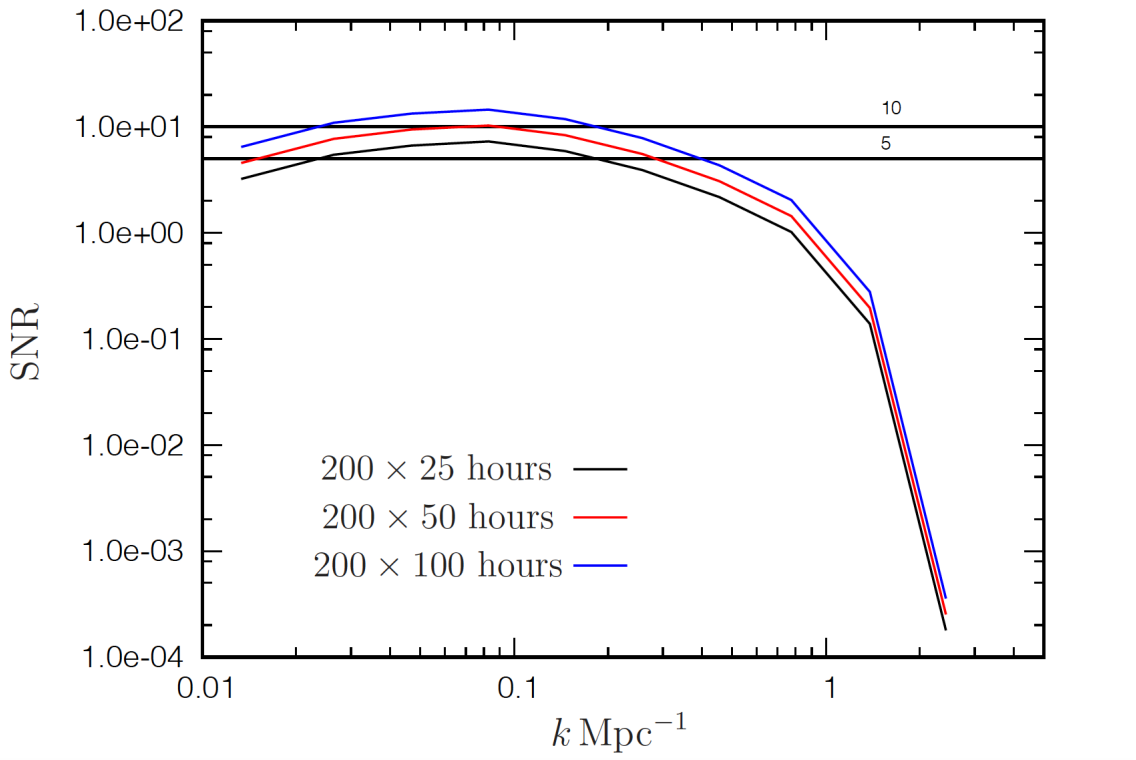

Figure 5.1: Shows the SNR for measuring the WDM cross power spectrum $P_{\mathcal{T}T}^{\mathrm{WDM}}(k)$ in different k-bins with observations of 200 hours each in $N_{\mathrm{p}} = 25$, 50 and 100 different fields-of-view. We have used a value of $m_{\mathrm{WDM}} = 0.25$ keV for this analysis. The lower and upper horizontal lines in the figure correspond to SNR = 5 and 10 respectively.

both the observations shall have different frequency resolutions, we have smoothed both the signals at the coarser resolution amongst the two.

5.4 Results

5.4.1 Predictions for the Ooty Wide Field Array (OWFA)

The OWFA is a linear radio-interferometric array that is expected to operate a central frequency of $\nu_c = 326.5\,\mathrm{MHz}$ (or, an wavelength of $\lambda_c = 0.9135$ m). This corresponds to observing the HI 21-cm radiation from a redshift $z_c = 3.35$ [229, 264]. The OWFA is a 530m long and 30m wide parabolic cylindrical reflector that is placed along the north south direction on a hill at a slope of 11°, which

is equal to the latitude of the place [265, 266]. This makes it possible to track a given part of the sky using a single rotation of the telescope about the telescope's long axis. The OWFA feed system consists of 1056 half-wavelength ($\sim 0.5\lambda_c$) dipoles, spaced 0.48 m equally apart, placed almost end-to-end along the long axis of the cyllinder. OWFA can operate in two independent simultaneous radio-interferometric modes - PI and PII [234]. The PI and PII respectively have 40 and 264 antennas in total, corresponding to the situations where signals from 24 dipoles and 4 dipoles have been added to make an single antenna element respectively. For the purpose of our analysis, we have only considered OWFA PII. The PII has the smallest and the largest baselines of 1.92 m and 505.0 m respectively. Both PI and PII have an operating bandiwdth of 39 MHz.

The possibility of detecting the HI 21-cm signal using OWFA has been studied extensively [234, 267–270]. Detailed foreground predictions [234, 271] and calibration issues [272] for OWFA have also been addressed.

5.4.1.1 The WDM power spectrum estimation using a visibility based approach to the cross-correlation

We begin our analysis by considering the possibility of constraining the shape of the cross power spectrum directly from future observations. To this end, we have assumed that the values of β_T and β_F are known a priori, and have considered constraining the shape of the cross power spectrum $P_{\mathcal{F}T}(k)$ (eq. 5.11) using observations of the cross-correlation signal with OWFA and an spectroscopic survey like SDSS-IV.

The prospects of measuring the binned cross power spectrum for the redshifts, $z_c = 3.35$, 3.05 and 2.55, and for the observing bandwidths, $B = 30$ and 60 MHz has been studied in an earlier work [273]. The study shows that we have the best possible measurement prospects of the binned cross power spectrum for the redshift and the bandwidth of 2.55 and 60 MHz respectively. In this work, we have considered observing the cross correlation signal at a redshift of 2.55 that corresponds to HI observation at a frequency of 400 MHz, and with a observing bandwidth of 60 MHz. Given this frequency and bandwidth, OWFA PII covers the k-range $0.010 \leq k \leq 3.13\,\mathrm{Mpc}^{-1}$. We have used a system temperature of $T_{\mathrm{sys}} = 100$ K to calculate the noise variance (eq. 3.4 in [273]) in our analysis.

As studied earlier in [273], the SNR for detecting the cross power spectrum grows rather slowly for observing time beyond 200 hours in a single field-of-view. This indicates that the SNR for observing time beyond 200 hrs in a single field-

of-view is dominated by the cosmic variance. It is therefore reasonable to consider carrying out observation of 200 hours each in N_p different independent pointing directions whereby the total observation time is, $T = 200N_p$. We have carried out our analysis with three different observing times, T = 5000, 10000 and 20000 hours that respectively correspond to observing in N_p = 25, 50 and 100 independent fields-of-view. For the purpose of the present analysis, we have binned the OWFA PII k-range into 10 equally spaced logarithmic k-bins. We have adopted the visibility based approach developed in [274] to study the prospects of detecting the WDM power spectrum using the cross correlation of Lyman-α forest and HI 21-cm signal with an upcoming radio-interferometric array OWFA and an spectroscopic survey like BOSS. We made the noise estimates using eqs. (3.10 - 3.14) in [273].

Figure 5.1 shows the predicted SNRs for measuring the cross power spectrum (eq. 5.11) in different k-bins for $m_{\rm WDM} = 0.25$ keV. We expect the measurement errors to be dominated by the cosmic variance at small k whereas at large k, the errors are predominantly due to the system noise.We find that it is possible to have a measurement of the cross power spectrum with SNR ≥ 5 in a number of bins within the range $0.02 \leq k \leq 0.2\,{\rm Mpc}^{-1}$ with an observation of 200 hours each in $N_p = 25$ different fields-of-view. For observations with $N_p = 50$ fields-of-view, we find that it is possible to have a measurement with SNR ≥ 5 for a number of bins within the range $0.015 \leq k \leq 0.25\,{\rm Mpc}^{-1}$. Measurement with an SNR in excess of 10 is possible in a single bin centred at $k = 0.08{\rm Mpc}^{-1}$. Prospects improve further if we consider observation with even more fields-of-view, $N_p = 100$, where it is possible to have a measurement with SNR ≥ 5 for a number of k-bins at $k < 0.4\,{\rm Mpc}^{-1}$. Measurement with SNR ≥ 10 is even possible in three k-bins within the range $0.02 \leq k \leq 0.15\,{\rm MPc}^{-1}$. The results do not vary significantly if we consider carrying out our analysis with smaller $m_{\rm WDM}$ values, $m_{\rm WDM} = 0.20$, 0.15 and 0.10 keV. We here emphasize that in the limit where the SNR is dominated by the cosmic variance, the noise is roughly proportional to the signal itself, whereby the SNR remains insensitive to the signal.

We now consider the prospects of the joint measurement of the two parameters, $\Omega_{\rm WDM}$, the warm dark matter density parameter, and $\Omega_{\Lambda 0}$, the dark energy density parameter marginalizing over the amplitude of the cross power spectrum. We have considered observations of the cross correlation signal for 200 hours each in 100 different fields-of-view. Figure 5.2 shows the relative errors in the joint measurement of $\Omega_{\rm WDM}$ and $\Omega_{\Lambda 0}$ for $m_{\rm WDM} = 0.25$ keV. We see that the errors in

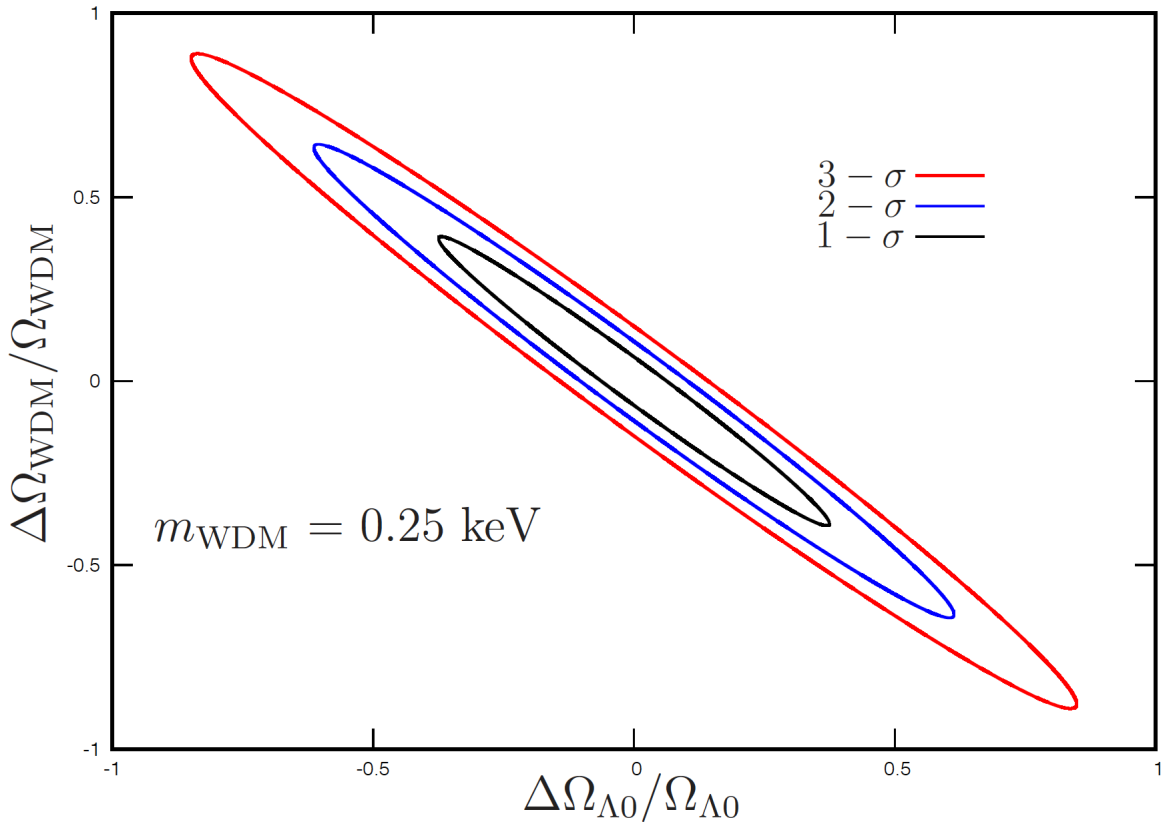

Figure 5.2: Shows the relative $1-\sigma$, $2-\sigma$ and $3-\sigma$ errors on the joint measurement of $\Omega_{\rm WDM}$ and $\Omega_{\Lambda 0}$ with an observing time of 200 hours each in $N_{\rm p} = 100$ different fields-of-view for $m_{\rm WDM} = 0.25$ keV.

the measurements of the parameters are anti-correlated. The relative errors in the measurement of both the parameters are roughly the same, the relative $1-\sigma$, $2-\sigma$ and $3-\sigma$ measurement errors are respectively ~ 0.4, ~ 0.6 and ~ 0.8. We have also considered carrying out the analysis with $m_{\rm WDM} = 0.20$ and 0.15 keV where we find that the errors increase slightly as the value of $m_{\rm WDM}$ is decreased.

As discussed earlier, we expect the WDM power spectrum to be suppressed on small scales. We here focus on the possibility of measuring the suppression in the WDM power spectrum in different k-bins using observations of the cross-correlation signal of 200 hours each in 100 different fields-of-view. By measuring this suppression with a high level of accuracy, one would be able to distinguish between the WDM and CDM cross power spectrum. The suppression in the WDM cross power spectrum is expected to be effective beyond a certain k, say k_{WDM}. It is therefore meaningful to bin the k-modes with $k \geq k_{WDM}$ in multiple k-bins and rest of the k-modes ($k < k_{WDM}$) in k-bin, and to consider measuring the WDM power spectrum in these k-bins. The suppression is expected to be prominent at large k. One may therefore hope to distinguish between the WDM and the CDM power spectrum only if the error on the measurement of the WDM power spectrum in the bin corresponding to larger k is small compared to the suppression in that k-bin. We see that for $m_{\rm WDM} = 0.25$ keV, $k_{WDM} \sim 0.1$ Mpc^{-1}. For the present purpose, we have divided the entires k-range into three different k-bins, k-modes with $k \leq 0.1$ Mpc^{-1} are lumped into a single k-bin, and we have divided the rest of the k-range ($0.1 \leq k \leq 3.13$ Mpc^{-1}) into two equispaced logarithmic k-bins. The left panel of figure 5.3 shows the predicted errors on the measurement of the WDM cross power spectrum for $m_{\rm WDM} = 0.25$ keV using 200 hours of observing time each in 100 different fields-of-view. We find that the errors on the measurement of the WDM power spectrum are ~ 7 and ~ 2.5 times smaller compared to the suppression of the WDM cross power spectrum in the two k-bins corresponding to the larger k-values. This refers to a measurement of the suppression at an confidence level of $6.9-\sigma$ and $2.5-\sigma$ respectively in two k-bins over the k-range $0.1 \leq k \leq 3.13$ Mpc^{-1}.

The suppression in the WDM power spectrum is relatively large for small $m_{\rm WDM}$ as compared to the larger $m_{\rm WDM}$. This encourages us to consider the possibility of improving the prospects of measuring the suppression by lowering $m_{\rm WDM}$. We here note that the value of the k_{WDM} decreases as $m_{\rm WDM}$ is lowered. However, we have held the k-ranges corresponding to the three different k-bins fixed for the rest of our analysis. Ther predicted errors on the measurement of the

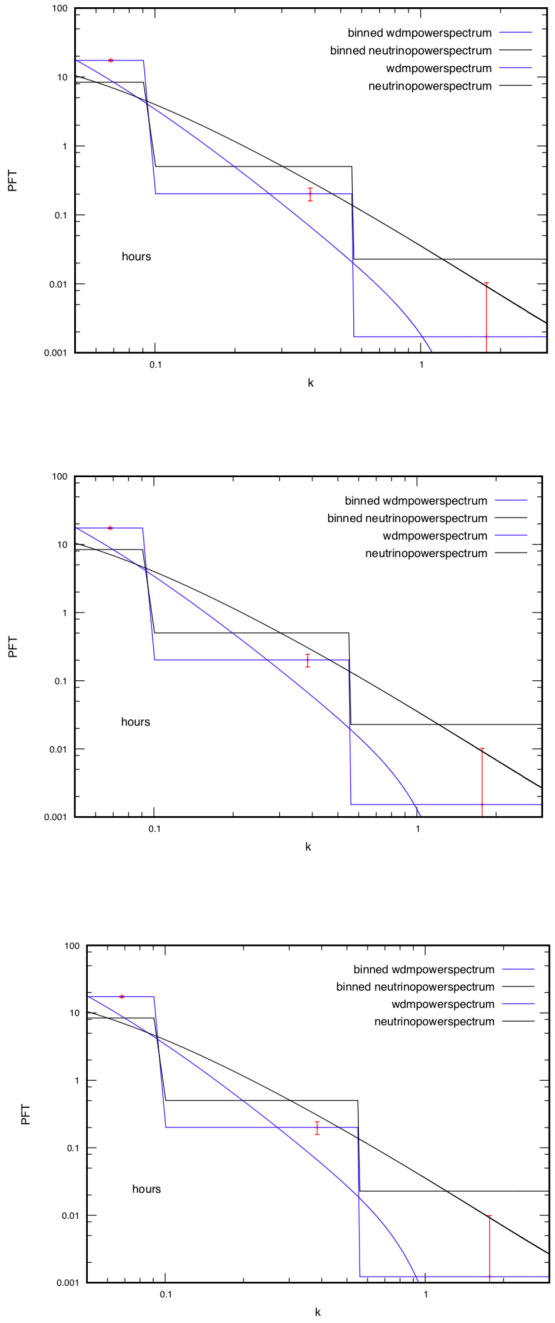

Figure 5.3: Shows the $1-\sigma$ errors (in red) on the measurement of the WDM cross power spectrum $P_{\mathcal{FT}}^{\rm WDM}(k)$ in two different k-bins with an observing time of 20000 hours distributed uniformly in $N_{\rm p}=100$ different fields-of-view. The upper, middle and lower panels in the figure show the results for the cases of $m_{\rm WDM}=$ 0.20, 0.15 and 0.10 keV respectively. The WDM (blue line) and the matter (black line) cross power spectrum are plotted for the binned WDM (blue horizontal steps) and CDM (black horizontal steps) cross power spectrum respectively.

WDM cross power spectrum is shown in the central and right panels of figure 5.3 respectively for $m_{\rm WDM} = 0.20$ and 0.15 keV. We find that errors decrease slightly, by factors of 1.01 and 1.04, and 1.04 and 1.08 in the two k-bins corresponding to the larger k-values respectively for $m_{\rm WDM} = 0.20$ and 0.15 keV. This corresponds to measuring the suppression at confidence levels of $7-\sigma$ and $2.6-\sigma$, and $7.2-\sigma$ and $2.7-\sigma$ in these two k-bins over the k-range $0.1 \leq k \leq 3.13$ Mpc^{-1} respectively for $m_{\rm WDM} = 0.20$ and 0.15 keV.

5.4.2 Predictions from SKA I mid

The baseline coverage of OWFA is small owing to the linear nature of the array. We now consider a radio-interferometric array for the 21-cm observation similar to the SKA1-mid. We have used the specifications of the radio telescope given in the 'Baseline Design Document'. We consider an interferometer with a total of 250 antennae each of which has a diameter of 15m. The range of operational frequencies is 350MHz to 14GHz. The baseline distribution of the array is obtained by assuming that 40%, 55%, 70% and 100% of the total number of antennae are within a radius of 0.35 km, 1 km, 2.5 km and 100 km respectively. We also assume that below a radius of 30m there is no baseline For our analysis we have assumed a system temperature $T_{sys} = 70$K. We have also assumed the bandwidth of the telescope to be 32MHz and an average antenna efficiency of 0.7 The formalism used in [248] is used to compute the SNR and make Fisher matrix estimates for WDM mass.

For a single pointing observation of the cross-correlation signal with the instrument as described above, the SNR improves very sluggishly beyond 400 hrs observations and saturates to a maximum of 3 (peak in k-space) for a 20000 hr observation which corresponds to the cosmic variance limit. Thus it is not worthwhile to consider 20000hr observation in a single field of view. Prospects of higher SNR is possible if the observation time is divided over many fields of view. This also maximally utilizes Lyman-alpha spectra available for cross-correlation.

The figure 5.4 shows the SNR for the cross-correlation signal for a fiducial WDM mass of $m_{WDM} = 0.25keV$ for observation time of 400 hrs 2000 hrs and 10000 hrs in a single pointing observation. The Lyman-alpha observational parameters are held fixed for this analysis. We find that if we consider a total observation time of 20000 hrs divided over multiple pointings then a peak SNR of $\sqrt{50} \times 1.6 = 9.9$, $\sqrt{10} \times 2.2 = 6.34$ and $\sqrt{2} \times 2.7 = 3.81$ is achievable in each of the cases respectively. The peak in SNR shifts in the k-space for different observation times but it is in

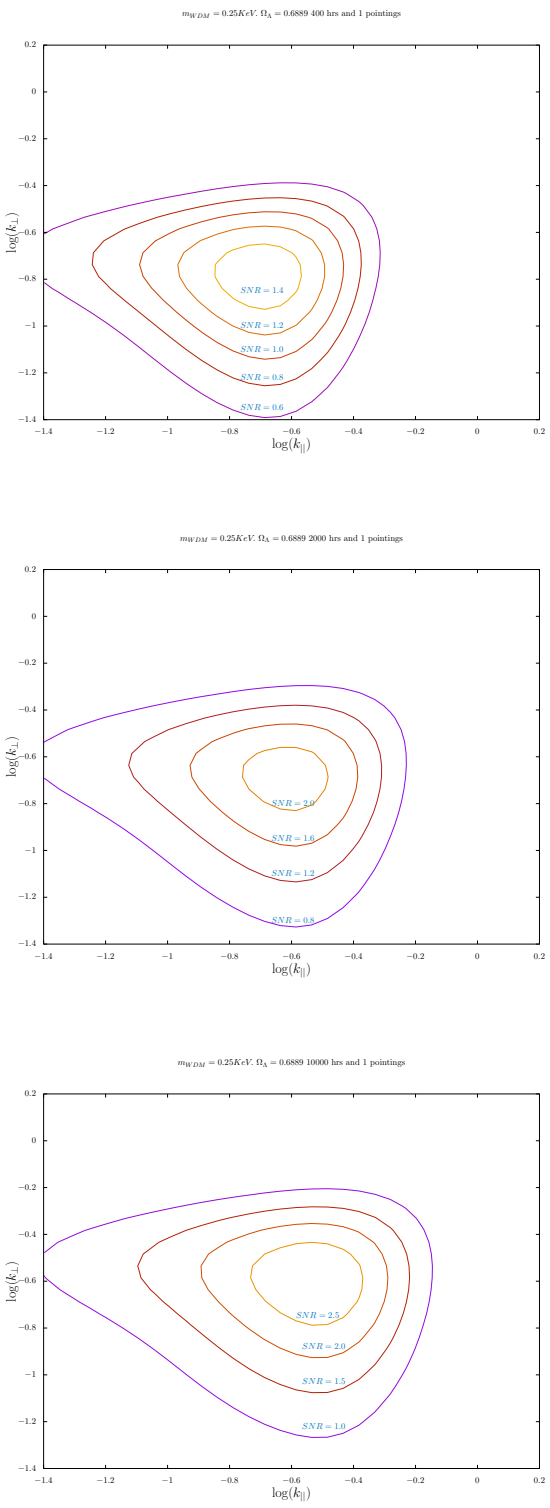

Figure 5.4: Figure showing the SNR for measuring the suppression in cross correlation power spectrum for a fiducial $m_{WDM} = 0.25$Kev for a single pointing 21 cm observation for 400hrs, 2000hrs and 10000hrs respectively.

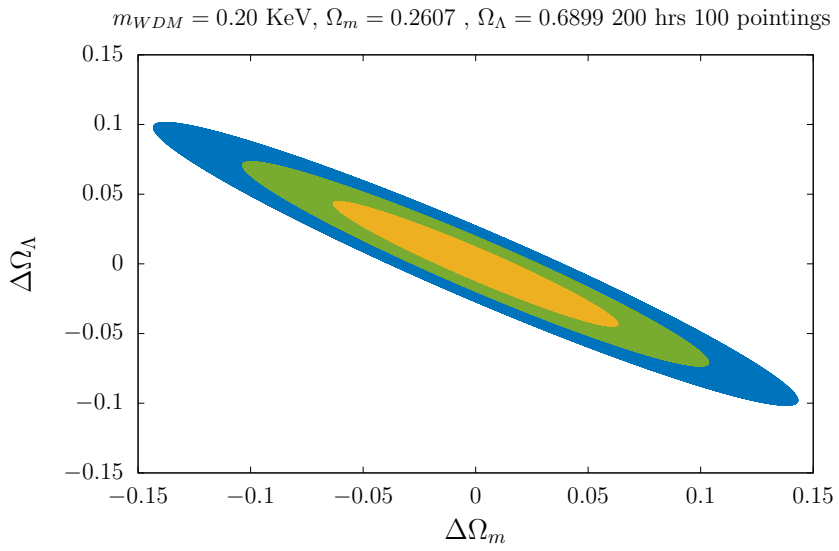

Figure 5.5: Figures showing the 68.3%, 95.4% and 99.8% error contours for Ω_{WDM} and Ω_Λ

the typical range $0.1\text{Mpc}^{-1} < \text{k} < 0.39\text{Mpc}^{-1}$.

The figure 5.5 shows the 68.3%, 95.4% and 99.8% error contours for the joint estimation of Ω_{WDM} and Ω_Λ. We have used the Fisher matrix formalism [248] to obtain the error ellipse. We consider a 20000 hr observation in 100 pointings each of duration 200 hrs. We find that for a fiducial WDM mass of 0.2 keV, the 1-σ relative error in Ω_{WDM} is ~ 0.16. We also note that Ω_Λ is constrained at $\sim 7\%$.

5.5 Conclusion

In this chapter we have investigated the possibility of constraining WDM mass using the cross-correlation of the redshifted HI 21-cm signal and the Lyman-α forest from the post-reionization epoch. The effect of WDM on the suppression of the matter power spectrum has the effect of enhancement of the 21-cm power spectrum through a non-linear bias which is large on small scales owing to the low abundance of small mass halos. We have considered a spectroscopic survey of the quasars with a mean quasar number density of $\bar{\text{n}}_\text{Q} = 48$ deg^{-2} over a survey area of 14455 deg^2, and a mean spectroscopic SNR = 5. We have chosen two futuristic radio-interferometers for our cross-correlation analysis namely OWFA and SKA1-mid. These two telescopes differ in their array layout and thereby in their baseline distribution. The former is a linear one-dimensional array and the latter is laid out in two dimensions.

Chapter 5: Constraining WDM power spectrum using cross-correlation of 21 cm and the Ly-α forest

Our analysis with OWFA shows that it is possible to measure the WDM power spectrum in several k-bins with SNR > 5 using an observation of 200 hours each in 100 different fields-of-view for $m_{\rm WDM} = 0.25$ keV. The relative $1-\sigma$ error in measurement of the parameter $\Omega_{\rm WDM}$ is ~ 0.8 for a fiducial $m_{\rm WDM} = 0.25$ keV. It is also possible to have a measurement of the suppression of power from the Cold Dark Matter (CDM) power spectrum at a confidence level of $\sim 7.2-\sigma$ and $\sim 2.7-\sigma$ in two different k-bins over the k-range $0.1 \leq k \leq 3.13$ Mpc^{-1} for $m_{\rm WDM} = 0.15$ keV. Considering a cross-correlation with SKA1-mid, we find that for a fiducial $m_{\rm WDM} = 0.25$ Kev, the suppression in the cross power spectrum can be measured at $\sim 10-\sigma$ around $k \sim 0.2$Mpc^{-1} for a total observing time of 20000 hrs distributed uniformly over 50 independent pointings. In summary, our study indicates that the cross-correlation of Lyman-α and post-reionization 21 cm signal maybe effective in putting cosmological bounds on WDM theories with far less severity of observational issues like foreground subtraction and systematics.